Impact of Sodium on the Water Dynamics in Prussian Blue Analogues

Citation for the original published paper (version of record):
Nielsen, I., Ulander, A., Jurànyi, F. et al (2024). Impact of Sodium on the Water Dynamics in Prussian Blue Analogues. Chemistry of Materials, 36(22): 11246-11253.
http://dx.doi.org/10.1021/acs.chemmater.4c02326

(article starts on next page)

CHEMISTRY OF MATERIALS

pubs.acs.org/cm
Article

Impact of Sodium on the Water Dynamics in Prussian Blue Analogues

Ida Nielsen,* Alexandra Ulander, Fanni Juranyi, Simon Rosenqvist Larsen, Maths Karlsson, William R. Brant, and Mikael S. Andersson*

Cite This: *Chem. Mater.* 2024, 36, 11246−11253

Read Online

ACCESS | Metrics & More | Article Recommendations | Supporting Information

ABSTRACT: Prussian blue analogues (PBAs) are interesting cathode materials for sodium-ion batteries, especially the iron-based, $[Fe(CN)_6]^{n-}$ vacancy-free PBA $Na_{2-x}Fe[Fe(CN)_6]\cdot zH_2O$. However, the presence of water has an opposing role in the application of PBAs as electrode materials: the water provides structural stability ensuring minimum volume changes during sodium extraction and insertion, however, water can react with the electrolyte leading to unwanted side reactions. Therefore, water must be replaced with another compatible small molecule to ensure optimal performance. To achieve this, insights into the dynamics of water are crucial. Two samples with compositions of $Na_{1.90(9)}Fe^{2+}_{0.90(7)}Fe^{3+}_{0.10(3)}[Fe^{2+}(CN)_6]\cdot 2.12(2)H_2O$ and $Na_{0.34(5)}Fe^{3+}[Fe^{2.66(5)+}(CN)_6]\cdot 0.360(4)H_2O$ were investigated using quasi-elastic neutron scattering (QENS). The results show that the water dynamics strongly depend on the sodium content. The water was found to diffuse within a spherical cavity in the porous framework with a radius of 2.6 Å for the high sodium-containing sample and 1.8 Å for the low sodium-containing sample consistent with the pore sizes in the crystal structures. In addition to the water diffusing within the pores, it was found that a small fraction of the water exhibits a rattling or rotational motion suggesting that this water strongly interacts and binds to the sodium ions. For the high sodium-containing sample, this rattling or rotational motion transforms into quantum rotational tunneling of the water below 75 K. These results give new fundamental insight into the role of water in PBAs, laying the groundwork for substituting water with another small molecule compatible with nonaqueous battery systems while also ensuring structural stability.

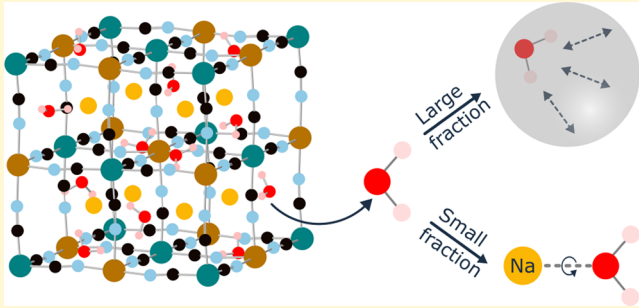

1. INTRODUCTION

As the demand for batteries continues to rise, the search for cheap, non-toxic, and abundant materials becomes increasingly essential. Prussian blue analogues (PBAs) are a material class widely researched as the positive electrode in sodium-ion batteries since they fulfill the required criteria. In particular, the iron-based, vacancy-free, sodium-containing PBA, $Na_{2-x}Fe[Fe(CN)_6]\cdot zH_2O$, is an attractive material because of its high theoretical capacity (171 mAh/g for x, $z = 0$) comparative to current lithium-ion technologies such as $LiFePO_4$.[1] The porous framework makes it possible to insert (extract) sodium ions during electrochemical cycling, while the nitrogen-bound high-spin iron and carbon-bound low-spin iron are reduced (oxidized) (Figure 1). Sodium-based PBAs adopt different structures depending on the sodium and water contents.[2] Initially, the hydrated material has a monoclinic structure (space group $P2_1/n$), which upon dehydration transforms to a rhombohedral structure (space group $R\bar{3}$) coinciding with a ∼20% reduction in the volume.[3] Removal of sodium from the dehydrated material leads to a transformation to cubic symmetry (space group $Fm\bar{3}m$) and a volume expansion of ∼17%, which can induce particle cracking. The large volume changes are avoided during sodium extraction and insertion in the hydrated material, thereby minimizing the risk of particle cracking. Thus, the presence of water provides structural stability,[4] however, its presence is highly damaging in nonaqueous battery systems due to side reactions with the electrolyte. Therefore, water must be replaced with another compatible molecule to stabilize the structure and allow PBAs to reach their full potential as electrode materials. Knowledge about the water dynamics in PBAs, *i.e.*, long-range vs localized processes, gives insights into which other guest molecules to consider. For example, localized processes are favored for structural stability since the guest molecule stays within the structure during ion extraction/insertion. However, to enable guest molecule exchange, some long-range diffusion is required. In addition, the new guest molecule should not

Received: August 19, 2024
Revised: November 8, 2024
Accepted: November 8, 2024
Published: November 16, 2024

https://doi.org/10.1021/acs.chemmater.4c02326
Chem. Mater. 2024, 36, 11246−11253

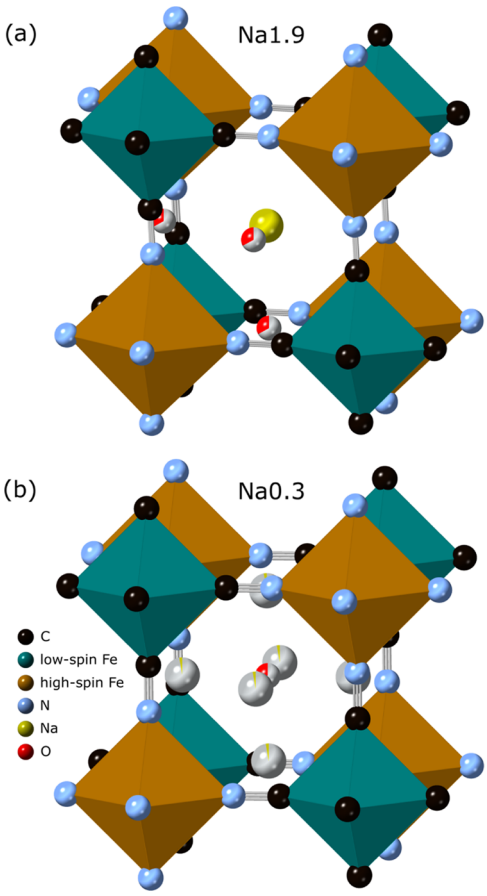

Figure 1. Local structure of (a) Na1.9 and (b) Na0.3 showing the position of sodium and oxygen within one subcube of the PBA framework. Sodium and oxygen are shown with partial occupancies based on the compositionally determined values.

bind strongly to sodium to avoid the molecule being extracted during sodium extraction (and possibly not reinserted again).

As the $[Fe(CN)_6]^{n-}$ (where n equals 3 or 4) vacancy content is low (leading to fewer sites to bind water) and the concentration of the alkali cations is high, the dynamics of the water molecules and the thermal behavior are expected to be very different from the previously studied Prussian blue $Fe[Fe(CN)_6]_{0.75}\cdot zH_2O$.[5] For Prussian blue, the water molecules exhibit local diffusion inside the large cavities created by the $[Fe(CN)_6]^{4-}$ vacancies (Figure S1). The water dynamics decreased if such vacancies were removed as in ferriferricyanide, $Fe[Fe(CN)_6]\cdot zH_2O$.[5] In both cases, water was found to undergo localized diffusion within a sphere with different cavity radii matching the pore sizes within the structures of the two materials. There were no signs of long-range diffusion in PB and ferriferricyanide. The water dynamics in iron-based, vacancy-free, and sodium-containing PBAs have never been studied before. Previous neutron diffraction (ND) studies of the structure of the material with a high sodium content showed that water exhibits several different orientations implying water dynamics.[3] Due to the structural changes upon desodiation, the dynamics might differ as a function of the sodium content, however, the water in the low sodium-containing sample is expected to have similar dynamic behavior as in ferriferricyanide.[5]

Here, we used quasi-elastic neutron scattering (QENS) to probe the dynamics of water in iron-based, vacancy-free PBAs. Two samples were prepared to study the water dynamics as a function of the sodium content and the temperature. One sample contained a high sodium content of $Na_{1.90(9)}Fe^{2+}_{0.90(7)}Fe^{3+}_{0.10(3)}[Fe^{2+}(CN)_6]\cdot 2.12(2)H_2O$ (Na1.9), while the other had a low sodium content of $Na_{0.34(5)}Fe^{3+}[Fe^{2.66(5)+}(CN)_6]\cdot 0.360(4)H_2O$ (Na0.3), thereby covering the two compositional extremes of the sodium content (Figure 1). The dynamic behavior of the water molecules in the two samples was extracted and related to their structures. Most of the water was found to move within a spherical cavity with decreasing cavity size as the sodium content decreased, while a small fraction of the water exhibited a rattling or rotational motion due to the interaction with sodium. Understanding the nature of the water dynamics (*e.g.*, local or long-range) is important for designing chemically modified PBAs where water is substituted with a molecule better suited for battery applications.

2. METHODS

2.1. Synthesis. The as-synthesized powder was obtained from Altris AB and used as received (denoted as Na1.9). To make a sample with a low sodium content, part of the Na1.9 sample was desodiated using oxygenated water followed by a second desodiation step involving NO_2BF_4. The first oxidation step was performed with water to decrease the chemical damage of the particles (surfaces, kinks, and other reactive surfaces) since water is less oxidative. Using NO_2BF_4 directly on the as-synthesized material results in less effective oxidation as NO_2BF_4 is consumed through the reaction with water. Dehydrating the as-synthesized material first will lead to particle cracking and loss of crystallinity,[3] which is undesirable. Oxygen dissolved in water can be described as a mild oxidizing agent with an oxidation potential of 3.11 V against Na/Na^+ yielding a sodium content of ∼1 sodium-ion per formula unit (f.u.). Oxidation with water and oxygen was achieved by putting 5.0 g of Na1.9 in 1 L of water while continuously stirring and bubbling with air. This was left for 5 days. The powder was filtered and dried to remove all water from the surface and crystal bulk (150 °C for 15 h). To further desodiate, NO_2BF_4 was used in a 4:1 molar ratio of NO_2BF_4/water oxidized powder (4 g of NO_2BF_4 and 2.16 g of the water oxidized powder). The water oxidized powder was added to 30 mL of acetonitrile in a Nalgene bottle, and the NO_2BF_4 was added. The solution was mixed for 10 min and then left to sediment. When sedimented (up to 3 days), approximately 20 mL of acetonitrile was removed with a syringe, and 20 mL of new acetonitrile was added. This procedure was repeated three times after which all acetonitrile was removed. The atmosphere was kept inert (N_2) during the entire synthesis. Finally, the Nalgene bottle containing the sample was dried in a Buchi oven to remove any remaining acetonitrile (85 °C for 20 h). The resulting sample (denoted as Na0.3) was left for hydration in a fumehood for 2−3 days. Details about the reaction mechanisms can be found in the Supporting Information.

To ensure that only crystal water was present in the samples (since the different kinds of water in PBAs cannot be distinguished in a QENS experiment), both samples were surface dried in a Buchi oven at 80 °C for 15 h.[6,7]

2.2. Compositional Characterization. Inductively coupled plasma-optical emission spectroscopy (ICP-OES) was used to determine the relative Na and Fe contents, and elemental analysis was used to determine the C, N, and H contents. The measurements were performed by Medac Ltd., U.K. Thermogravimetric analysis (TGA) was performed on TA Instruments TGA5500 instrument to determine the water content. Around 5 mg of powder was placed on a platinum pan that was placed in the furnace. The samples were heated from room temperature to 500 °C with a heating rate of 5 °C per min under flowing N_2 (25 mL/min). The water content was determined in the temperature range of 30−250 °C since all water is expected to be gone by 250 °C.[6,7] Mössbauer spectroscopy was performed to determine the ratio of the two iron sites, *i.e.*, the $[Fe(CN)_6]^{n-}$ vacancy

https://doi.org/10.1021/acs.chemmater.4c02326
Chem. Mater. 2024, 36, 11246−11253

content in the samples. In addition, the sodium content can indirectly be estimated from the iron valences. The measurements were carried out at room temperature on a spectrometer with a constant acceleration type of vibrator and a ^{57}CoRh source. The samples were enclosed in a sealed aluminum cover to form an absorber with a sample concentration of ~7 mg/cm^2. Calibration spectra were recorded at 295 K using a natural Fe metal foil as a reference absorber. The spectra were folded and fitted using the least-squares Mössbauer fitting program Recoil to obtain the values of the center shift CS, the magnitude of the electric quadrupole splitting |QS|, the full-width at half-maxima W of the Lorentzian absorption lines, and the spectral areas A.

2.3. X-Ray and Neutron Diffraction. In-house X-ray diffraction (XRD) was performed on a Bruker D8 Powder diffractometer (double Cu Kα radiation λ_1 = 1.540600 Å and λ_2 = 1.5444390 Å) with a Lynxeye XE-T position sensitive detector. The samples were placed on a powder holder surrounded by a Si disk, and the experiments were performed between 10 and 80° with a step size of 0.02°.

Variable temperature synchrotron X-ray diffraction was performed on the Na1.9 sample at the DanMAX beamline at the MAX IV Laboratory in Lund, Sweden. The sample was packed in a 0.3 mm borosilicate capillary inside an argon-containing glovebox. The data were collected with a wavelength of 0.6199 Å and a Dectris Pilatus3 2 M CdTe area detector. The temperature was varied between 85 and 500 K with a heating rate of 5 K/min using an Oxford Cryostream 800+.

Neutron diffraction (ND) data were collected on the time-of-fight instrument POLARIS[8] at the ISIS Pulsed Neutron and Muon Source.[9,10] Around 1.0 g of each sample was loaded into 8 mm cylindrical vanadium cans inside an argon-containing glovebox and sealed using indium wire. The experiments were conducted at room temperature for 1.5 h.

The XRD and ND patterns were refined in Topas Academic V6.[11] The structures were visualized using CrystalMaker.[12]

2.4. Quasi-Elastic Neutron Scattering. Quasi-elastic neutron scattering experiments were performed on the cold neutron direct geometry time-of-flight spectrometer FOCUS at SINQ, Switzerland.[13] The samples were packed inside an argon-containing glovebox by evenly distributing the powders (1.45 g for Na0.3 and 0.97 g for Na1.9) in an aluminum foil bag optimized to allow for 90% neutron transmission to minimize multiple neutron scattering. The bag was folded into a cylindrical shape and inserted into an annular aluminum can with a diameter of 12 mm (two bags for Na0.3) sealed with lead wire. The QENS experiments were conducted in the temperature range of 45−330 K using a closed-cycle refrigerator and a wavelength of 6 Å (Q range of 0.4−1.8 Å^{-1}). The instrument's resolution was determined to be ~0.04 meV by collecting spectra from a vanadium standard at room temperature. QENS measurements were performed at 45, 150, 250, and 330 K for sample Na0.3 and at 45, 50, 60, 75, 90, 105, 150, 200, 280, and 330 K for sample Na1.9.

The obtained quantity from a QENS experiment is the scattering function, which can be described in general with the following function:

$$S(Q, \omega) \sim R(Q, \omega) \otimes [\delta(\omega)A_{\mathrm{E}}(Q) + \sum L_i(\omega)A_{\mathrm{QE},i}(Q)] \quad (1)$$

where ω is the angular frequency of the neutrons, δ is the delta function used to describe the elastic scattering, L_i are the Lorentzian functions used to describe the quasi-elastic scattering, and A_{E} and $A_{\mathrm{QE},i}$ are the areas corresponding to the delta and Lorentzian functions, respectively. The data were reduced and fitted in the DAVE software.[14] The Q binning was performed such that the sample Bragg peak at Q = 1.20 Å^{-1} was avoided. By fitting the data to eq 1 using two Lorentzian functions, the elastic and quasi-elastic contributions were extracted, and the elastic incoherent structure factor (EISF) was estimated using the following relationship:

$$\mathrm{EISF} = \frac{A_{\mathrm{E}}(Q)}{A_{\mathrm{E}}(Q) + \sum A_{\mathrm{QE},i}(Q)} \quad (2)$$

The reorientational dynamics were determined by comparing the experimentally determined EISF to EISF models, which consider both local and long-range dynamics.

3. RESULTS AND DISCUSSION

3.1. Composition and Structure. The composition of the samples was determined to be $Na_{1.90(9)}Fe^{2+}_{0.90(7)}Fe^{3+}_{0.10(3)}[Fe^{2+}(CN)_6]\cdot 2.12(2)H_2O$ (Na1.9) and $Na_{0.34(5)}Fe^{3+}[Fe^{2.66(5)+}(CN)_6]\cdot 0.360(4)H_2O$ (Na0.3) from TGA and Mössbauer spectroscopy confirming PBA samples with no $[Fe(CN)_6]^{n-}$ vacancies and a high and low sodium content, respectively. Details for the TGA and Mössbauer measurements can be found in the Supporting Information Table S2 and Figures S2, S3. The reduction in the water content as the sodium content is lowered follows previously observed trends for iron-based, $[Fe(CN)_6]^{n-}$ vacancy-free PBAs.[6,15] ICP-OES analysis revealed similar sodium content for Na0.3 as determined by Mössbauer spectroscopy, while the results implied the presence of a sodium-containing impurity in Na1.9 (Table S1).[15] Based on previously reported water and sodium contents for samples similar to Na1.9,[6,15] the impurity is not believed to contain hydrogen and/or iron. Thus, the impurity will not affect the QENS results reported here since QENS is dominated by the large incoherent scattering cross section of hydrogen, which is present only in the main phase. The determined compositions are similar to previous reports on high and low sodium content, vacancy-free, iron-based PBAs.[15] The structure of the samples was determined after the synthesis using laboratory XRD. The sample Na1.9 consists of mainly a rhombohedral phase (88.7(7)%, space group $R\bar{3}$) with a minor cubic phase (11.3(7)%, space group $Fm\bar{3}m$) possibly due to a slight oxidation of the powder (Figure S4). The sample Na0.3 has a face-centered cubic structure (space group $Fm\bar{3}m$). The low-temperature synchrotron XRD patterns of Na1.9 show a monoclinic structure (space group $P2_1/n$) at 85 K, which converts to a rhombohedral structure above 280 K (Figure S5). The structural relationship between $P2_1/n$ and $R\bar{3}$ is described in detail in a previous study.[3] It should be noted that there is negligible change in the cavities within the structures during this phase transition, and therefore, it does not significantly change the water environment.

Neutron diffraction was employed to accurately determine the structure and position of water within the PBA framework in the two samples. The structure of Na1.9 was modeled using $R\bar{3}$ symmetry (Figure S6, Table S3). The minor $Fm\bar{3}m$ phase was not included in the refinement because of the very hkl-dependent peak shape of this phase. However, the addition of the $Fm\bar{3}m$ phase or exclusion of the high-resolution detector bank (where this phase is mainly present) did not affect the refinement outcome for the $R\bar{3}$ phase. After the PBA framework and the position of sodium were determined, Fourier difference maps were used to locate the position of oxygen (water). The Fourier difference map indicated one oxygen position (Figure S7), which was included in the model with the water content fixed to the value obtained from TGA. The final model resulted in an acceptable fit and reasonable refined parameters similar to previously reported high sodium content, iron-based PBAs.[3] However, the refined atomic displacement parameter (ADP) for the oxygen atom was

https://doi.org/10.1021/acs.chemmater.4c02326
Chem. Mater. 2024, 36, 11246−11253

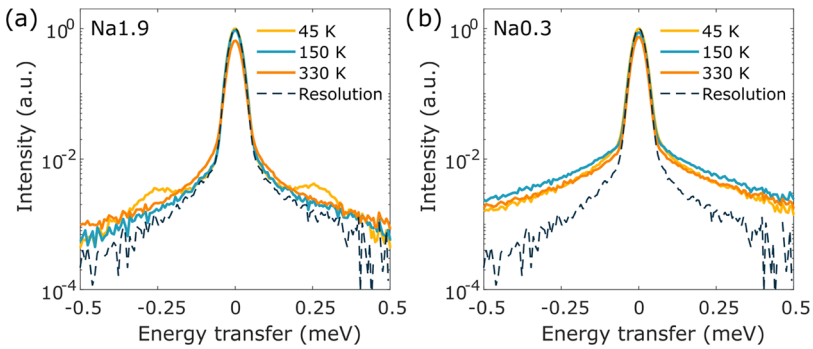

Figure 2. QENS spectra at selected temperatures (Q = 1.6 Å^{-1} with a bin size of 0.4 Å^{-1}) for (a) Na1.9 and (b) Na0.3.

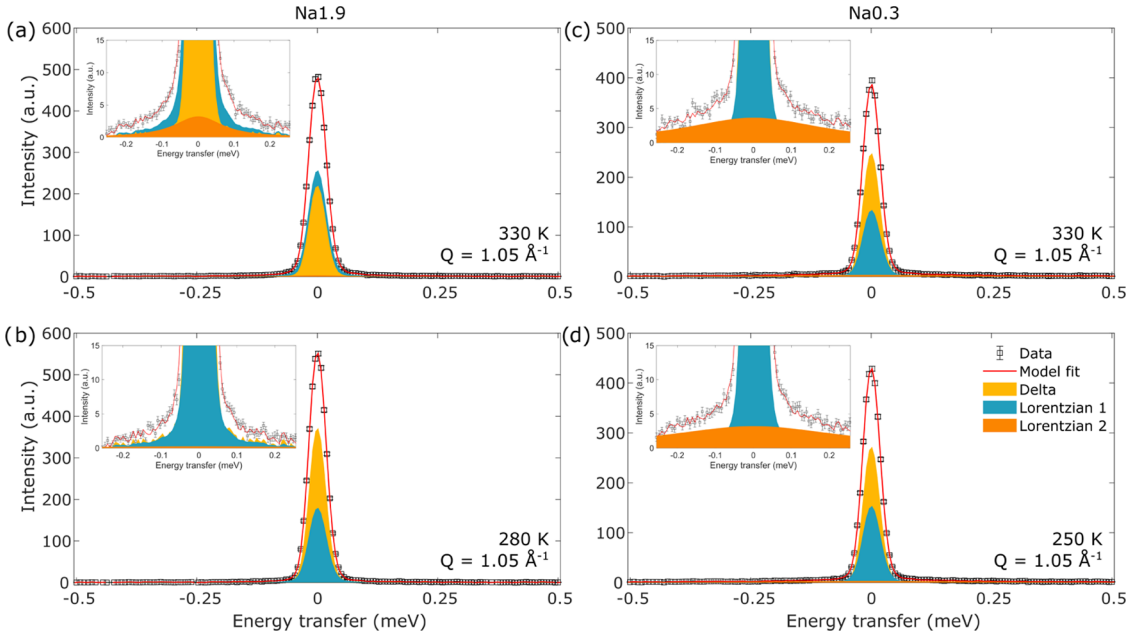

Figure 3. Fitted QENS spectra for (a, b) Na1.9 and (c, d) Na0.3 showing the individual components of the fit (Q = 1.05 Å^{-1} with a bin size of 0.1 Å^{-1}). The insets show the broad Lorentzian 2 (orange). The error bars are one standard deviation.

quite high, indicating positional disorder. The positional disorder indicates that water may exhibit dynamics, which can be captured by QENS and is discussed in Section 3.3. A lower ADP value could be obtained if the oxygen occupancy was refined, however, this resulted in a much lower water content (1.2 H_2O per f.u. vs 2.12 H_2O per f.u.), which is unreasonable based on the water content determined from TGA. This outcome could possibly be due to the presence of the second phase, which may contain water and was not included in the refinement. The oxygen atoms are located on three of the six faces of a subcube surrounded by the iron atoms and cyanide ligands between the sodium ions (Figures 1a and S1b). Similar to previous work, a model with oxygen occupying all six faces of each subcube did not fit the data, and this model was thus discarded.[3]

The structure of Na0.3 was modeled using $Fm\bar{3}m$ symmetry (Figure S8, Table S4). Here, Fourier difference maps were initially used to locate the positions of sodium and oxygen, however, because of the higher symmetry, there are larger uncertainties in the Fourier difference maps. Thus, different positions of sodium and oxygen were tested and evaluated based on the refined ADPs, positions, and occupations. The best model has sodium ions located close to the faces of the subcube while oxygen (water) occupies the center of the subcube (Figure 1b). The sodium and water contents were fixed to the values obtained from ICP-OES and TGA. Comparing the structure of the two samples, the reduction of the sodium content results in the sodium ions migrating toward the faces of the subcubes leading the water to occupy the center of the subcube. This agrees with theoretical predictions[16] and is similar to the structure of ferriferricyanide, which contains no sodium ions but only water in the structure placed in the center of the subcube.[17]

3.2. General Observations of the QENS Spectra. For both samples, quasi-elastic broadening is observed in the investigated temperature range of 45−330 K (Figure 2) with the broadening being more pronounced for Na0.3. The broadening is attributed to the hydrogen atoms of the water molecules in the samples since the incoherent scattering contribution from the other elements (iron, sodium, nitrogen, carbon, and oxygen) is 2% for Na1.9 and 7% for Na0.3. Noteworthy, dynamics are still present even at 45 K for both samples. For Na1.9, two satellite peaks are observed in the QENS spectra recorded at 45 K suggesting quantum rotational tunneling of the water molecules at this temperature. The tunneling is discussed in detail in Section 3.4.

https://doi.org/10.1021/acs.chemmater.4c02326
Chem. Mater. 2024, 36, 11246−11253

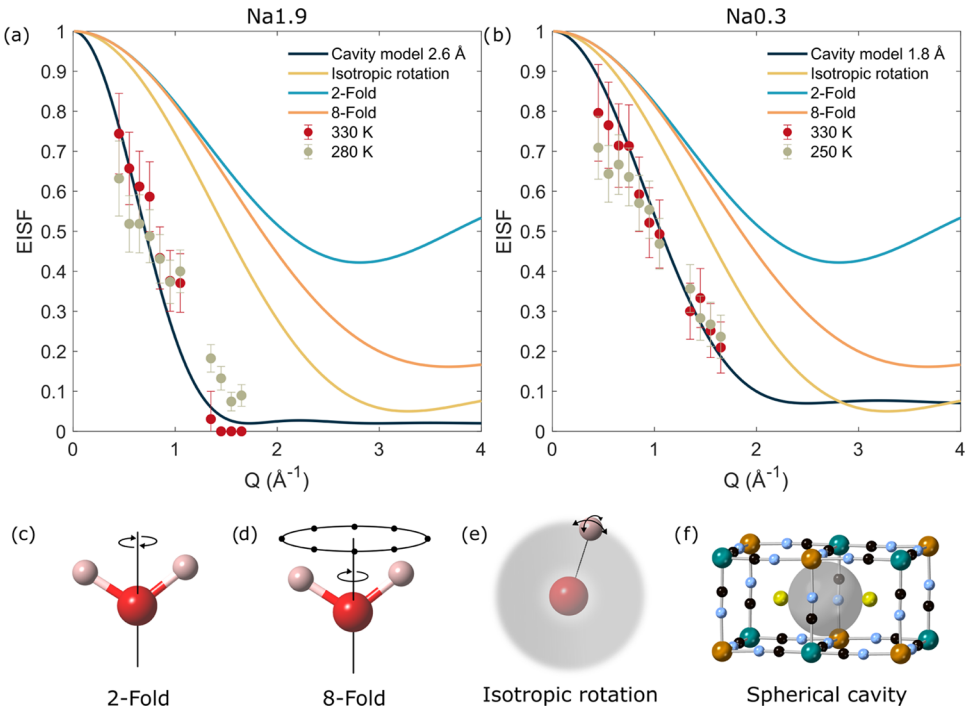

Figure 4. EISFs determined from the QENS spectra for (a) Na1.9 at 330 and 280 K and (b) Na0.3 at 330 and 250 K. The error bars are two standard deviations. (c−f) Representations of common reorientational motions for water molecules. (c) 2-fold rotation around the C_2-axis. (d) 8-fold rotation around the C_2-axis. (e) Isotropic rotation model with the hydrogen atoms moving in a sphere around oxygen's center of gravity. (f) Spherical cavity model where the water molecule can diffuse within a cavity of a certain size. The incoherent contribution from other elements in the sample was calculated to be 2% for Na1.9 and 7% for Na0.3 and is accounted for in the EISF cavity model.

Fitting of the spectra using eq 1 revealed that two Lorentzian functions are needed to describe the quasi-elastic broadening: one narrow and one broad component. The widths of the two Lorentzians were determined by fitting data of a single Q bin (1.4−1.8 Å^{-1}). These widths were used to fit spectra over the entire Q range (0.4−1.7 Å^{-1}) and accurately describe the spectra at each Q value. The spectra with Q values of 1.15 and 1.25 Å^{-1} were removed from the fit due to contamination from a sample Bragg peak at Q = 1.20 Å^{-1}. Representative fits of the spectra are shown in Figure 3. The fact that the data can accurately be described by two Lorentzians with fixed widths over the entire Q range suggests that the water dynamics are of local character, such as rotational motion (*i.e.*, not long-range translational motion). The two Lorentzians used to describe the data suggest different dynamics for the water molecules with either different time scales or types of motion. The width of the broad Lorentzian (Lorentzian 2 in Figure 3) is 100 times larger than the width of the narrow Lorentzian (Lorentzian 1 in Figure 3), *e.g.*, 0.15(1) meV for Lorentzian 2 vs 0.004(1) meV for Lorentzian 1 for Na1.9 at 330 K (Table S5). The area of the broad Lorentzian (Lorentzian 2) is ∼6% of the area of the narrow Lorentzian (Lorentzian 1) at Q = 1.65 Å^{-1} meaning that only a small fraction of the water is contributing to the broad Lorentzian. This motion is attributed to water most likely being coordinated to sodium resulting in a rattling or rotation around the 2-fold axis, *i.e.*, the sodium−oxygen axis. Because this is a small fraction of water, it is not possible to experimentally confirm this motion from this data. On the other hand, the area of the narrow Lorentzian (Lorentzian 1) changes as a function of Q and is therefore associated with local diffusion of the water molecules. The width of Lorentzian 1, related to local diffusion, is lower than previously observed for Prussian blue and ferriferricyanide, where no sodium is present.[5] Thus, the presence of sodium appears to reduce the speed of the water dynamics in the PBAs. However, it should be noted that the width of the narrow Lorentzian curve is close to the limit of the resolution of the spectrometer. Therefore, it was only possible to fit the two highest temperatures for each sample since the width of Lorentzian 1 became too narrow upon cooling. To probe the dynamics stemming from the narrow component at lower temperatures, QENS studies using a spectrometer with a higher energy resolution are required, however, this is outside of the scope of this study. Nevertheless, fitting the QENS spectra using only the broad component is not sufficient to describe all of the quasi-elastic broadening (Figure S10). Since this broad component is seen for both samples, it is not believed to originate from the minor $Fm\bar{3}m$ phase observed for Na1.9 nor the sodium-containing impurity in this sample (Table S1).

3.3. Water Diffusion. After extracting the elastic and quasi-elastic contributions from the data, the experimental EISFs were determined (Figure 4a,b) and compared to several EISF models for water dynamics with the mathematical expressions provided in the Supporting Information. The presence of the broad Lorentzian (Lorentzian 2) does not affect the calculated EISF (Figure S9) and is thus neglected. The experimental EISFs were compared to four different EISF models.[5] The first EISF model describes the 2-fold rotation of the hydrogen atoms around the C_2-axis (Figure 4c). The second EISF model describes the 8-fold rotation (as a representation of a many-fold rotation) around the C_2-axis (Figure 4d). The third EISF model describes the isotropic rotation of the hydrogen atoms around the water molecule's center of gravity (Figure 4e). The last EISF model describes the diffusion of the water molecule inside a sphere with a specific radius (Figure 4f).[18]

https://doi.org/10.1021/acs.chemmater.4c02326
Chem. Mater. 2024, 36, 11246−11253

All experimental EISFs agree well with a spherical cavity model, while the data cannot be described by the local rotation of the water molecule. The sizes of the cavities were determined by fitting the EISF model to the experimental EISF data while considering possible cavities in the structure of the samples. For Na1.9, a cavity with a radius of 2.6 Å was determined from the EISF fits and can be found in the structure between the two sodium ions between two subcubes (Figure 4f). This agrees with the average structure determined from neutron diffraction, where the oxygen atom is positioned on the face of the PBA subcube with a Na−O distance of 2.610(8) Å. Water's diffusion within a spherical cavity of a few Å agrees with the positional disorder found for oxygen in the structural model. The determined cavity radius of 2.6 Å is similar to PB,[5] however, the cavity is relocated to be in between the sodium ions as compared to PB where the cavity is created by the $[Fe(CN)_6]^{n-}$ vacancies in the structure.[5] This suggests that the presence of sodium does not restrict the movement of water within the structure. For Na0.3, a cavity with a radius of 1.8 Å was determined from the EISF fits. Relating this to the structure of the sample, a cavity with a radius of ∼2.1 Å can be found between water and sodium in the center of the subcube (Figure 1b). The flexible PBA framework, resulting in local distortions of each subcube, combined with the presence of sodium might contribute to a smaller effective cavity within each subcube. It is implied that sodium and water occupy a subcube simultaneously since the QENS and ND data suggest a smaller cavity size than if water was alone in a subcube. In addition, for sodium- and iron-based PBAs, the water content strongly depends on the sodium content. Thus, when lowering the sodium content, the water content is also lowered[6,15] indicating a strong interaction between sodium and water to stay together inside the structure. The determined cavity radius of 1.8 Å for Na0.3 from the EISF fitting is similar to the cavity radius of 1.85 Å previously found for ferriferricyanide.[5] In contrast to earlier findings, there is no temperature evolution of the EISF for these samples. However, this might be due to the relatively small temperature range probed since the dynamics become slower than the resolution of the spectrometer at lower temperatures.

To further verify that most of the water performs local diffusion within a cavity, the spectra were fitted using the incoherent scattering law for diffusion within a sphere with a cavity radius a.[18]

$$S_s(Q, \omega) \sim A_0^0(Q)\delta(\omega) + \frac{1}{\pi} \sum_{\{l,n\}\neq\{0,0\}} (2l+1) A_n^l(Q) \frac{(x_n^l)^2 D/a^2}{[(x_n^l)^2 D/a^2]^2 + \omega^2} \quad (3)$$

In contrast to the above section, where the experimental EISF was only compared to the EISF for diffusion within a cavity, the data are now directly fitted with eq 3 using the first six Lorentzians. In this model, the widths can be calculated numerically only for a given value of a and D. The width of the quasi-elastic broadening is related to the diffusion coefficient $D = \frac{\mathrm{FWHM}_n^l \cdot a^2}{2\cdot(x_n^l)^2}$, where FWHM is the full-width at half-maximum for each Lorentzian, and x_n^l is the dimensionless parameter relating the widths and areas. By fitting the incoherent scattering law directly to the data, a more restricted fitting approach is applied since the only fitting parameters are the area (A_n^l) and the width of the narrowest Lorentzian, which then are related to the other Lorentzians through x_n^l (Figure S11). The value of a is fixed to the determined cavity sizes from the EISF fits in Figure 4a,b, while the fraction of incoherent scattering from other elements is fixed to 2% for Na1.9 and 7% for Na0.3 (as in Figure 4a,b). Figure S12 shows the fit of the QENS spectra using the incoherent scattering law for diffusion within a sphere. The first six Lorentzians in the model cover 97.8% and 99.3% of the total scattering (Q = 1.55 Å^{-1}) for Na1.9 and Na0.3, respectively. Similar to the QENS fits in Figure 3, a broad Lorentzian was added as the background in the fitting. All quasi-elastic broadening can be described well using this model with the respective cavity radii (2.6 Å for Na1.9 and 1.8 Å for Na0.3), and the refined widths are in the same order of magnitude as found for the QENS fits in Figure 3, *e.g.*, 0.45(9) meV for the Lorentzian background and 0.00208(6) meV for the cavity model for Na1.9 at 330 K. The diffusion constant D was estimated using eq 3 and is 3.92 × 10^{-8} cm^2/s for Na1.9 and 2.17 × 10^{-8} cm^2/s for Na0.3. The small change in D between the two samples is most likely a consequence of the limited space in Na0.3 relative to that in Na1.9. Thus, the data suggest that water diffuses inside a spherical cavity where the size of the cavity decreases with decreasing sodium content.

3.4. Tunneling. As mentioned earlier, satellite peaks in the QENS spectra for Na1.9 at 45 K were observed indicating quantum rotational tunneling. Therefore, the temperature evolution of this phenomenon was investigated (Figure 5). The two tunneling peaks move toward the elastic peak when

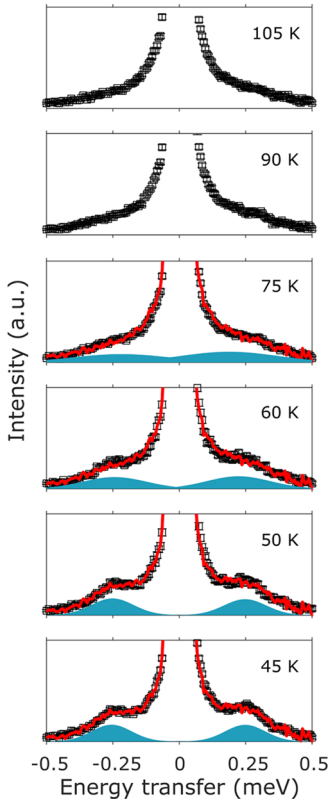

Figure 5. Fitted QENS spectra of the tunneling as a function of the temperature for Na1.9. The individual components of the fits are shown in blue. The error bars are one standard deviation.

https://doi.org/10.1021/acs.chemmater.4c02326
Chem. Mater. 2024, 36, 11246−11253

the temperature is increased. By 90 K, the tunneling peaks are indistinguishable from the typical quasi-elastic broadening meaning that the dynamics of the hydrogen atoms are thermally activated jumps over the rotational barrier rather than tunneling through the rotational energy barrier. Usually, quantum rotational tunneling is observed at much lower temperatures[19] suggesting that the features observed here would be more pronounced at lower temperatures. Such satellite peaks in the QENS spectra could also arise from a magnetic transition due to the presence of iron in the sample. However, the temperature-dependent magnetization of Na1.9 shows no magnetic transitions upon cooling to 10 K (Figure S14). The possibility of an ortho−para transition of the water molecule[20] is also excluded since there are no changes in the intensity of the satellite peaks as a function of time as expected for an ortho−para transition. The tunneling energy is quite high (meV scale while tunneling often occurs at μeV scale[19]) suggesting that the rotational barrier of the water molecules is very small. The QENS spectra containing tunneling peaks were fitted with a delta function and two Gaussian functions, one for each tunneling peak. The tunneling EISF was determined by comparing the tunneling peak areas with the area of the delta function (Figure S13). Since the tunneling EISF is close to 1, it is clear that only a small fraction of the water molecules are involved in the tunneling. Due to the low fraction of tunneling water, the tunneling EISF contains large error bars making it impossible to determine a Q dependence. Since there is no broad component in the tunneling temperature range, the tunneling water could be the same fraction of water contributing to the broad Lorentzian (Lorentzian 2 in Figure 3), *i.e.*, the rattling or rotational motion around the sodium−oxygen axis. Quantum rotational tunneling was not observed for Na0.3 and has not been observed for other PBAs previously. The tunneling energies are very sensitive to the local environment of water indicating that it strongly depends on the PBA composition and structure. Nevertheless, sample Na0.3 could potentially have tunneling at temperatures lower than those probed in this study. The energy barrier for tunneling can be investigated with inelastic neutron scattering probing the librations of the water molecules, which have a similar energy barrier.

4. CONCLUSIONS

To ensure structural stability during ion insertion and extraction and a long lifetime of PBA electrode materials, it is necessary to replace water with another compatible molecule. Quasi-elastic neutron scattering experiments on iron-based, vacancy-free PBAs with either a high or low sodium content were performed to gain insights into the water dynamics, which are directly correlated to the stabilizing effect water has on the structure. The water dynamics were of local character with most of the water diffusing within a spherical cavity of a few Å consistent with the pore sizes within the structures. Furthermore, there were no signs of long-range diffusion of the water. The cavity radius for the high sodium-containing sample is similar to the previously studied Prussian blue (2.6 Å), but the cavity is instead placed in between the sodium ions. Thus, the insertion of sodium does not restrict the movement of water within the structure. Upon removal of sodium, the cavity radius decreased to 1.8 Å similar to the previously studied ferriferricyanide. Quantum rotational tunneling of a small fraction of the water molecules was found for the sample with a high sodium content below 75 K, while it was absent in the sample with a low sodium content in the investigated temperature range. For the low sodium-containing sample, there was a rattling or rotational motion still present at 45 K. This further shows that the water dynamics in PBAs are composition-dependent and highly dependent on the local structure. These results show that if water is to be replaced with another small molecule compatible with nonaqueous battery systems, it should not necessarily have a specific geometry but instead exhibit localized dynamics filling out the pores in the structure thereby stabilizing the structure, not binding strongly to sodium, and not containing any protic hydrogen. Acetonitrile is a possible candidate molecule that may fulfill the above criteria. This work provides important information about the water dynamics in PBAs and lays the groundwork for what other small molecules with which water can be substituted. This knowledge can also be applied to PBAs used in other applications, such as gas absorption and catalysis, where the interaction among the PBA framework, alkali cations, and neutral guest species is important for their performance.

■ ASSOCIATED CONTENT

Supporting Information

The Supporting Information is available free of charge at https://pubs.acs.org/doi/10.1021/acs.chemmater.4c02326.

Synthesis, sample characterization, refinements details, fitted QENS spectra and their EISF, and magnetization data (PDF)

■ AUTHOR INFORMATION

Corresponding Authors

Ida Nielsen − *Department of Chemistry—Ångström Laboratory, Uppsala University, SE-751 21 Uppsala, Sweden;* orcid.org/0000-0002-6511-8291; Email: ida.nielsen@kemi.uu.se

Mikael S. Andersson − *Department of Chemistry—Ångström Laboratory, Uppsala University, SE-751 21 Uppsala, Sweden;* orcid.org/0000-0002-7119-0951; Email: mikael.andersson@kemi.uu.se

Authors

Alexandra Ulander − *Department of Chemistry—Ångström Laboratory, Uppsala University, SE-751 21 Uppsala, Sweden*

Fanni Juranyi − *Laboratory for Neutron Scattering, Paul Scherrer Institute, CH-5232 Villigen, Switzerland;* orcid.org/0000-0002-3223-072X

Simon Rosenqvist Larsen − *Department of Chemistry—Ångström Laboratory, Uppsala University, SE-751 21 Uppsala, Sweden;* orcid.org/0000-0002-8107-4110

Maths Karlsson − *Department of Chemistry and Chemical Engineering, Chalmers University of Technology, SE-412 96 Göteborg, Sweden;* orcid.org/0000-0002-2914-6332

William R. Brant − *Department of Chemistry—Ångström Laboratory, Uppsala University, SE-751 21 Uppsala, Sweden*

Complete contact information is available at: https://pubs.acs.org/10.1021/acs.chemmater.4c02326

Author Contributions

I.N.: Conceptualization, validation, formal analysis, investigation, data curation, writing—original draft, writing—review and editing, visualization, and project administration. A.U.: Investigation and resources. F.J.: Methodology, validation,

formal analysis, and investigation. S.R.L.: Validation, investigation, and writing—review and editing. M.K.: Conceptualization, validation, supervision, and writing—review and editing. W.R.B.: Conceptualization, validation, resources, writing—review and editing, supervision, and funding acquisition. M.S.A.: Conceptualization, methodology, validation, formal analysis, investigation, data curation, writing—review and editing, visualization, and supervision.

Notes

The authors declare the following competing financial interest(s): W.R.B. is a co-founder of the company Altris AB, which provided the as-synthesized powder (the Na1.9 sample) used in this study.

■ ACKNOWLEDGMENTS

This research is funded by Stiftelsen för Strategisk Forskning (SSF) within the Swedish National Graduate School in Neutron Scattering, SwedNess (GSn15-0008). W.R.B. acknowledges funding from the Strategic Research Area StandUp for Energy and Energimyndigheten (45517-1). M.S.A. acknowledges support from the ÅForsk Foundation grant no. 21-453 and the Göran Gustafsson Foundation. A.U. acknowledges support from Vetenskapsrådet (2021-04987). Experiments at the ISIS Neutron and Muon Source were supported by beamtime allocation XB2291005 and XB2291006 from the Science and Technology Facilities Council. I.N. acknowledges Paul F. Henry for doing the neutron diffraction experiments. This work is based on experiments performed at the Swiss spallation neutron source SINQ, Paul Scherrer Institute, Villigen, Switzerland. We acknowledge MAX IV Laboratory for time on BeamLine DanMAX under Proposal 20221283. Research conducted at MAX IV is supported by the Swedish Research council under contract 2018-07152, the Swedish Governmental Agency for Innovation Systems under contract 2018-04969, and Formas under contract 2019-02496. DanMAX is funded by the NUFI grant no. 4059-00009B. Mads Amdisen is acknowledged for performing the variable temperature synchrotron X-ray diffraction experiments, and Tore Ericsson, Lennart Häggström, and Fredrik Lindgren are acknowledged for performing the Mössbauer experiments and analysis.

■ REFERENCES

(1) Gao, X.; Liu, H.; Deng, W.; Tian, Y.; Zou, G.; Hou, H.; Ji, X. Iron-based layered cathodes for sodium-ion batteries. *Batteries Supercaps* **2021**, *4*, 1657−1679.

(2) Boström, H. L. B.; Brant, W. R. Octahedral tilting in Prussian blue analogues. *J. Mater. Chem. C* **2022**, *10*, 13690−13699.

(3) Nielsen, I.; Dzodan, D.; Ojwang, D. O.; Henry, P. F.; Ulander, A.; Ek, G.; Häggström, L.; Ericsson, T.; Boström, H. L. B.; Brant, W. R. Water driven phase transitions in Prussian White cathode materials. *J. Phys. Energy* **2022**, *4*, No. 044012.

(4) Guo, X.; Wang, Z.; Deng, Z.; Li, X.; Wang, B.; Chen, X.; Ong, S. P. Water contributes to higher energy density and cycling stability of Prussian blue analogue cathodes for aqueous sodium-ion batteries. *Chem. Mater.* **2019**, *31*, 5933−5942.

(5) Sharma, V. K.; Mitra, S.; Thakur, N.; Yusuf, S. M.; Juranyi, F.; Mukhopadhyay, R. Dynamics of water in prussian blue analogues: Neutron scattering study. *J. Appl. Phys.* **2014**, *116*, No. 034909.

(6) Ojwang, D. O.; Häggström, L.; Ericsson, T.; Angström, J.; Brant, W. R. Influence of sodium content on the thermal behavior of low vacancy Prussian white cathode material. *Dalton Trans.* **2020**, *49*, 3570−3579.

(7) Ojwang, D. O.; Häggström, L.; Ericsson, T.; Mogensen, R.; Brant, W. R. Guest water hinders sodium-ion diffusion in low-defect Berlin green cathode material. *Dalton Trans.* **2022**, *51*, 14712−14720.

(8) Smith, R. I.; Hull, S.; Tucker, M. G.; Playford, H. Y.; McPhail, D. J.; Waller, S. P.; Norberg, S. T. The upgraded Polaris powder diffractometer at the ISIS neutron source. *Rev. Sci. Instrum.* **2019**, *90*, No. 115101.

(9) Xpress Access beamtime at the ISIS Neutron and Muon Source (XB 2291005, 2291006) was provided by the UK Science and Technology Facilities Council (STFC) DOI: 10.5286/ISIS.E.RB2291005-1.

(10) Xpress Access beamtime at the ISIS Neutron and Muon Source (XB 2291005, 2291006) was provided by the UK Science and Technology Facilities Council (STFC) DOI: 10.5286/ISIS.E.RB2291006-1.

(11) Coelho, A. A. TOPAS and TOPAS-Academic: An optimization program integrating computer algebra and crystallographic objects written in C++. *J. Appl. Crystallogr.* **2018**, *51*, 210−218.

(12) Images and video generated using CrystalMaker: a crystal and molecular structures program for Mac and Windows. CrystalMaker Software Ltd., Oxford, England.

(13) Janßen, S.; Mesot, J.; Holitzner, L.; Furrer, A.; Hampelmann, R. FOCUS: A hybrid TOF-spectrometer at SINQ. *Phys. B* **1997**, *234*−*236*, 1174−1176.

(14) Azuah, R. T.; Kneller, L. R.; Qiu, Y.; Tregenna-Piggott, P. L.; Brown, C. M.; Copley, J. R.; Dimeo, R. M. DAVE: A comprehensive software suite for the reduction, visualization, and analysis of low energy neutron spectroscopic data. *J. Res. Natl. Inst. Stand. Technol.* **2009**, *114*, 341−358.

(15) Boras, D.; Nielsen, I.; Buckel, A.; Ericsson, T.; Häggström, L.; Younesi, R.; Stabb, T.; Brant, W. R. Determening internal porosity in Prussian blue analogue cathode materials using poistron annihilation lifetime spectroscopy. *J. Mater. Sci.* **2023**, *58*, 16344−16356.

(16) Wang, Y. P.; Hou, B. P.; Cao, X. R.; Wu, S. Q.; Zhu, Z. Z. Structural evolution, redox mechanism, and ionic diffusion in rhombohedral $Na_2FeFe(CN)_6$ for sodium-ion batteries: First-principles calculations. *J. Electrochem. Soc.* **2022**, *169*, No. 010525.

(17) Kumar, A.; Yusuf, S. M.; Keller, L. Structural and magnetic properties of $Fe[Fe(CN)_6]\cdot 4H_2O$. *Phys. Rev. B: Condens. Matter Mater. Phys.* **2005**, *71*, No. 054414.

(18) Volino, F.; Dianoux, A. J. Neutron incoherent scattering law for diffusion in a potential of spherical symmetry: General formalism and application to diffusion inside a sphere. *Mol. Phys.* **1980**, *41*, 271−279.

(19) Verdal, N.; Udovic, T. J.; Rush, J. J.; Stavila, V.; Wu, H.; Zhou, W.; Jenkins, T. Low-temperature tunneling and rotational dynamics of the ammonium cations in $(NH_4)_2B_{12}H_{12}$. *J. Chem. Phys.* **2011**, *135*, No. 094501.

(20) Goh, K. S. K.; Jiménez-Ruiz, M.; Johnson, M. R.; Rols, S.; Ollivier, J.; Denning, M. S.; Mamone, S.; Levitt, M. H.; Lei, X.; Li, Y.; Turro, N. J.; Murata, Y.; Horsewill, A. J. Symmetry-breaking in the endofullerene H2O@C60 revealed in the quantum dynamics of ortho and para-water: A neutron scattering investigation. *Phys. Chem. Chem. Phys.* **2014**, *16*, 21330−21339.